Constraining the influence of natural variability to improve estimates of global aerosol indirect effects in a nudged version of the Community Atmosphere Model 5

Gabriel J. Kooperman,[1] Michael S. Pritchard,[2] Steven J. Ghan,[3] Minghuai Wang,[3] Richard C. J. Somerville,[1] and Lynn M. Russell[1]

Received 30 July 2012; revised 17 October 2012; accepted 21 October 2012; published 11 December 2012.

[1] Natural modes of variability on many timescales influence aerosol particle distributions and cloud properties such that isolating statistically significant differences in cloud radiative forcing due to anthropogenic aerosol perturbations (indirect effects) typically requires integrating over long simulations. For state-of-the-art global climate models (GCM), especially those in which embedded cloud-resolving models replace conventional statistical parameterizations (i.e., multiscale modeling framework, MMF), the required long integrations can be prohibitively expensive. Here an alternative approach is explored, which implements Newtonian relaxation (nudging) to constrain simulations with both pre-industrial and present-day aerosol emissions toward identical meteorological conditions, thus reducing differences in natural variability and dampening feedback responses in order to isolate radiative forcing. Ten-year GCM simulations with nudging provide a more stable estimate of the global-annual mean net aerosol indirect radiative forcing than do conventional free-running simulations. The estimates have mean values and 95% confidence intervals of -1.19 ± 0.02 W/m^2 and -1.37 ± 0.13 W/m^2 for nudged and free-running simulations, respectively. Nudging also substantially increases the fraction of the world's area in which a statistically significant aerosol indirect effect can be detected (66% and 28% of the Earth's surface for nudged and free-running simulations, respectively). One-year MMF simulations with and without nudging provide global-annual mean net aerosol indirect radiative forcing estimates of -0.81 W/m^2 and -0.82 W/m^2, respectively. These results compare well with previous estimates from three-year free-running MMF simulations (-0.83 W/m^2), which showed the aerosol-cloud relationship to be in better agreement with observations and high-resolution models than in the results obtained with conventional cloud parameterizations.

Citation: Kooperman, G. J., M. S. Pritchard, S. J. Ghan, M. Wang, R. C. J. Somerville, and L. M. Russell (2012), Constraining the influence of natural variability to improve estimates of global aerosol indirect effects in a nudged version of the Community Atmosphere Model 5, *J. Geophys. Res.*, *117*, D23204, doi:10.1029/2012JD018588.

1. Introduction

[2] The addition of anthropogenic aerosol particles to Earth's atmosphere, through the burning of fossil fuels, industrial production, and land use changes, impacts the transmission of radiation not only by direct scattering and absorption, but also by indirect modifications to cloud properties. Aerosol-induced changes to cloud reflectivity, lifetime, and vertical positioning are known as "aerosol indirect effects," which project onto global scales as a planetary radiative forcing. Radiative forcing refers to any perturbation in the global-annual mean net radiative flux at the top of the atmosphere resulting from instantaneous changes in the amount of incoming or outgoing radiation. The Intergovernmental Panel on Climate Change Fourth Assessment Report (IPCC AR4) gave a best estimate of the radiative impact due to anthropogenic aerosol induced changes in cloud reflectivity as -0.70 [-1.1, $+0.4$] W/m^2 [*Forster et al.*, 2007].

[3] While the magnitude of the aerosol indirect effect is smaller and opposite to that of greenhouse gases (GHGs, 2.63 [± 0.26] W/m^2), it represents the largest source of uncertainty in estimates of the overall anthropogenic forcing (1.6 [-1.0, $+0.8$] W/m^2), nearly four times that of GHGs [*Forster et al.*, 2007]. Accurately determining the magnitude of individual components of the present-day anthropogenic

[1]Scripps Institution of Oceanography, University of California, San Diego, La Jolla, California, USA.
[2]Department of Atmospheric Sciences, University of Washington, Seattle, Washington, USA.
[3]Pacific Northwest National Laboratory, Richland, Washington, USA.

Corresponding author: G. J. Kooperman, Scripps Institution of Oceanography, University of California, San Diego, 9500 Gilman Dr., Dept. 0224, La Jolla, CA 92093-0224, USA. (gkooperman@ucsd.edu)

0148-0227/12/2012JD018588

radiative forcing is critical for improving projections of future climate, as well as for informing effective policy decisions concerning the climate impacts of human activities.

[4] Aerosol particles alter clouds through their role as cloud condensation and ice nuclei (CCN and IN) and through their thermodynamic effects on the ambient environment in which clouds form. Aerosol-driven droplet nucleation is evident from regional field observations [e.g., *Leaitch et al.*, 1992; *DeMott et al.*, 2003; *Andreae et al.*, 2004; *Kaufman et al.*, 2005] and from global satellite measurements [e.g., *Coakley et al.*, 1987; *Bréon et al.*, 2002] of forest fire emissions, desert dust plumes, ship tracks, and industrial pollution. Increases in the concentration of nucleating particles can result in smaller droplets, which more efficiently backscatter solar radiation and thus increase cloud albedo [*Twomey*, 1977]. Smaller droplets may also result in reduced precipitation efficiency and increased cloud lifetime [*Albrecht*, 1989]. Recent studies suggest that these effects depend strongly on cloud regime, and thus regional observations cannot be usefully extended to global estimates [*Stevens and Feingold*, 2009]. In some cases an opposite (positive) forcing is possible, if precipitation is enhanced by aerosol-induced convective invigoration [*Rosenfeld et al.*, 2008] or if cloud top height changes due to aerosol-modified atmospheric stability [*Wood*, 2007].

[5] The complex nature of these microphysical processes can result in both positive and negative forcings [*Lohmann and Feichter*, 2005] and thus contributes importantly to the large uncertainty shown in the 90% inter-model confidence intervals from the IPCC AR4 given above. Estimates of global aerosol effects from observations are further complicated by temporally intermittent emissions, inhomogeneous spatial distributions, and short residence times [*Rosenfeld and Feingold*, 2003]. While the most recent climate models now include physical processes that are important to many aerosol-cloud interactions, it can still be difficult to distinguish the statistically significant anthropogenic signal from the noise of natural variability and feedbacks in conventional simulations [*Stevens and Feingold*, 2009]. As increasing computational power enables modeling efforts to do more justice to the details of cloud-aerosol physical interactions, this signal-to-noise problem is likely to become more severe and thus will further increase uncertainty. Indirect effects are part of the overall cloud forcing, which is influenced by natural modes of variability on many timescales and by poorly understood cloud feedbacks [*Bony et al.*, 2006]. The transport, removal, and distribution of aerosol particles themselves are also strongly dependent on aspects of the circulation associated with natural variability [*Gong et al.*, 2006].

[6] Because the cloud lifetime effect involves changes in the cloud lifecycle it is not possible to estimate the effect in a single simulation. Thus, the traditional method for isolating the anthropogenic forcing in models is to compare two simulations with and without anthropogenic emissions after integrating them over the timescales of the dominant modes of natural variability [*Forster et al.*, 2007; *Lohmann and Feichter*, 2005; *North and Stevens*, 1998]. In this case, the simulations not only have different emissions, but they are also unconstrained meteorologically, i.e., they produce unique weather patterns that affect the cloud cover and cloud liquid water content – the same properties involved with the cloud lifetime effect. A signal in the overall mean difference is only statistically significant where it is larger than a metric of internal variability (i.e., standard inter-annual error), and in practice the signal is often weak in those parts of the world where natural variability is high or the signal of aerosol indirect effect is low [*Ming et al.*, 2005].

[7] By design, this approach requires long simulation times to produce the full range of variability governed by natural processes in the climate system. This is less a problem for conventionally parameterized climate models, which contain highly idealized cloud-aerosol physics in order to remain computationally affordable for long simulations. But this approach is a serious problem for climate models using embedded convection-resolving models to represent the physics of cloud-aerosol interactions more realistically (and whose predictions of aerosol indirect effects are therefore of special interest), because these more ambitious models are so computer-intensive that they require vast computing resources to produce long simulations.

[8] In summary, current estimates of aerosol indirect effects are complicated by approximations of cloud-aerosol physics, unconstrained meteorology, and poorly understood feedbacks. The modeling approach presented here aims to improve these estimates by implementing Newtonian relaxation (nudging) in the National Center for Atmospheric Research (NCAR) Community Atmosphere Model version 5 (CAM5) to constrain large-scale meteorology and to reduce differences in natural variability between simulations with pre-industrial and present-day aerosol emissions. Nudging here refers to the practice of adding a term to the prognostic model equations, proportional to the difference between a model-computed value of a variable, and an observed or prescribed value of that variable at the given space and time position. In this study, nudging forces the simulated winds and dry static energy to follow prescribed trajectories, thus controlling synoptic meteorology, circulation, and large-scale feedbacks so as to isolate the radiative influence of anthropogenic aerosol.

[9] Similar to the method of fixing surface temperature to remove feedback responses [*Shine et al.*, 2003], this nudging method effectively fixes the temperature response to the given forcing, but in the entire atmospheric column rather than just at the surface. This provides the additional benefit of more closely approximating aerosol indirect effects as an instantaneous or pure forcing. It also removes some of the challenges associated with distinguishing radiative forcing from feedbacks in conventional simulations, which otherwise require new metrics that account for climate sensitivity and/or "fast-feedback" processes, including: quasi-forcing [*Rotstayn and Penner*, 2001], stratospheric adjustment [*Forster et al.*, 1997], temperature-regressed radiative forcing [*Forster and Taylor*, 2006], and radiative flux perturbation [*Lohmann et al.*, 2010], in order to accurately compare the impact of aerosol relative to that of other anthropogenic forcing agents.

[10] The nudging approach is also shown to be a useful strategy to bring new modeling technology, which would otherwise be too computationally expensive, to bear on estimating aerosol indirect effects. Advances in aerosol-climate modeling on global scales have been achieved through increased resolution and the inclusion of more complex physical/chemical processes, which push the limit

of current computing hardware. One such model is the new Multiscale Aerosol Climate Model (MACM) developed at Pacific Northwest National Laboratory (PNNL) [*Wang et al.*, 2011a]. MACM is based on the multiscale modeling framework (MMF) approach pioneered by *Grabowski and Smolarkiewicz* [1999] and *Grabowski* [2001] and developed by the Center for Multiscale Modeling of Atmospheric Processes (CMMAP) in which an idealized cloud-resolving model (CRM) is embedded in each grid column of global climate model (GCM) to replace conventional statistical parameterizations [*Khairoutdinov and Randall*, 2001]. The MACM has extended the MMF approach to include the enhanced aerosol physics contained in CAM5. *Wang et al.* [2011a, 2011b, 2012] have shown that resolved convection in MACM improves simulated aerosol-cloud relationships, but at a high computational cost. Nudging not only reduces differences in natural variability between simulations, but also reduces the required simulation time to reach a stable estimate.

[11] Details of the GCMs and nudging approach used in this study are provided in Section 2, including discussion of relevant physical parameterizations. The experimental setup and prescribed model forcings are given in Section 3. An overview of the findings is presented in the Section 4. A summary and future work are given in Section 5.

2. Background

2.1. Model Description

2.1.1. Community Atmosphere Model

[12] CAM5 was run in this experiment as a stand-alone atmospheric general circulation model (AGCM) with an interactive land surface and prescribed sea surface temperatures and sea ice. The treatment of aerosol-cloud physics has undergone many notable updates in CAM5 relative to its predecessor, including the addition of a three-mode two-moment aerosol module, a two-moment cloud microphysics scheme, deep convection with vertical entrainment and convective momentum transport, shallow convection based on moist turbulent processes, and radiative transfer calculations from the Rapid Radiative Transfer Model for GCMs [*Neale et al.*, 2010]. For all simulations CAM5 was run with a finite volume dynamical core at a standard supported horizontal resolution of 1.9° latitude by 2.5° longitude ($\sim$200 $\times$ 200 km) and 30 hybrid sigma-pressure vertical levels. A short overview of physical processes relevant to this experiment is given here; for more details, see *Neale et al.* [2010].

[13] CAM5 includes an interactive three-mode aerosol module that separately transports and processes fifteen different aerosol constituents distributed into Aitken, accumulation, and coarse modes, as described by *Liu et al.* [2012], which is based on an earlier scheme tested in the Community Climate Model [*Easter et al.*, 2004] and CAM3 [*Ghan and Easter*, 2006]. The module not only evolves aerosol plumes as they are transported, but more importantly provides key linkages between simulated aerosol fields and microphysical cloud and radiation parameterizations that drive the hydrologic and energy cycles. Sulfate, black carbon, and primary organic matter particles are injected at various heights by direct emission inventories; sea salt and dust enter the atmosphere through mechanistic surface source parameterizations; and volatile organic compounds and gas phase sulfur are emitted and oxidized before forming secondary aerosol. Gas and aqueous phase processes involving bulk sulfur and secondary organic precursor gases add to the overall aerosol mass through both the creation of new Aitken mode particles and condensation onto existing particles in all three modes [*Easter et al.*, 2004].

[14] Aerosol particle evolution in the model includes nucleation, growth by condensation, coagulation, aqueous and gas phase production, and removal by wet and dry deposition [*Easter et al.*, 2004]. Number and mass mixing ratios for particles in each mode transition between interstitial and cloud-borne states as droplets form, evaporate, collide, and fall from the atmosphere. Aerosol activation (droplet nucleation) at cloud base is parameterized as a function of updraft velocity and aerosol mode properties [*Abdul-Razzak and Ghan*, 2000], which convert particles from a clear-air to cloud-borne state and impact cloud water through microphysical calculations [*Morrison and Gettelman*, 2008]. Vertical transport of interstitial and cloud-borne particles is driven by mass flux calculations from the Zhang-McFarlane and University of Washington parameterizations of deep and shallow convection, respectively [*Neale et al.*, 2010; *Park and Bretherton*, 2009; *Zhang and McFarlane*, 1995]. Particle removal by wet scavenging occurs both in and below clouds, and particles not re-suspended by cloud evaporation are removed through precipitation [*Easter et al.*, 2004].

[15] The aerosol module directly interacts with both the microphysical and radiative transfer schemes, impacting cloud formation and precipitation as well as direct light extinction and deposition changes to the surface albedo. CAM5 uses a two-moment bulk cloud microphysics scheme, which tracks mass mixing ratios and number concentrations of in-cloud and precipitating liquid and ice condensate. Condensate can undergo growth by condensation and collection, phase change due to freezing, melting, and evaporation, and sedimentation, all driven by sub-grid scale variability [*Morrison and Gettelman*, 2008]. Cloud droplet nucleation is consistent with Köhler theory [*Köhler*, 1936] of aerosol particle activation and is based on the three-mode distribution and aerosol chemical properties described above, as well as temperature, water vapor content, and vertical velocity [*Abdul-Razzak and Ghan*, 2000]. Mixed-phase cloud microphysics is treated using the ice nucleation parameterization of *Liu and Penner* [2005] and the *Liu et al.* [2007] treatment of supersaturation. Dust serves as an ice nuclei in CAM5 and sulfate influences homogeneous nucleation, which can produce significant impacts on ice clouds [*Ghan et al.*, 2012].

[16] Decomposition of the aerosol direct, indirect, and semi-direct effects of the shortwave and longwave energy balance simulated by CAM5 has been described by *Ghan et al.* [2012]. The analysis was based on the last five years of six-year free-running simulations.

2.1.2. Multiscale Modeling Framework

[17] Processes relevant to clouds occur on scales from micrometers to thousands of kilometers, and representing all of them with a single set of statistical parameterizations has proven extremely difficult [*Randall et al.*, 2003]. *Grabowski and Smolarkiewicz* [1999] presented a new approach through which, rather than diagnose cloud-scale processes from large-scale dynamics, they chose instead to embed

simplified two-dimensional cloud resolving models (CRMs) in each grid column of a GCM in order to explicitly represent sub-grid convection. *Khairoutdinov and Randall* [2001] first introduced this approach in CAM3, which later became known as a superparameterized GCM, also known as a multiscale modeling framework [*Randall et al.*, 2003]. In every GCM grid volume of such a model, CAM thus supplies each realization of the embedded CRM with a large scale forcing [*Benedict and Randall*, 2009]. A moist convective response is harvested from the CRM as a sub-grid update to CAM [*Grabowski*, 2001]. Radiative transfer is calculated through the CRM cloud field, which provides explicit sub-grid cloud overlap geometry, the lack of which introduces uncertainty in conventional GCM cloud parameterizations [*Khairoutdinov et al.*, 2005]. Independent CRMs with periodic boundary conditions make this model extremely scalable on current parallel computing hardware, bypassing the processor-to-processor communication bottleneck that limits the resolution of conventional GCMs [*Grabowski and Smolarkiewicz*, 1999; *Khairoutdinov et al.*, 2005]. The MMF is approximately two hundred times more computationally expensive than a conventionally parameterized GCM (such as CAM5), but it is still about a thousand times less expensive than a global CRM would be and is scalable with current computer architecture [*Khairoutdinov et al.*, 2005].

[18] The MMF approach has been promoted by a National Science Foundation (NSF) Science and Technology Center called CMMAP (www.cmmap.org), which has recently collaborated with PNNL to implement a new version of the model, based on CAM5, to better represent the multiscale interactions between aerosol and clouds [*Wang et al.*, 2011a]. In this new model, MACM, the microphysics module for the CRM has been updated to include a two-moment microphysics scheme consistent with the scheme introduced in CAM5 [*Morrison et al.*, 2005]. Aerosols are coupled with resolved cloud dynamics using an approach called the Explicit Cloud – Parameterized Pollutants (ECPP) method [*Gustafson et al.*, 2008]. ECPP links aerosol particles on the GCM grid to statistics of cloud properties from the CRM, and aerosol particle transport is explicitly represented by the vertical gradient of aerosol concentration and resolved CRM scale subsidence [*Gustafson et al.*, 2008]. Aerosol humidification is calculated from CRM relative humidity, improving the representation of sub-grid aerosol-radiation interactions. Similarly, aerosol activation into cloud droplets occurs on the CRM grid, so that within every GCM grid box an explicit distribution of cloud droplet number concentrations is calculated. Unlike in CAM5, aerosol particle concentrations are not directly linked to ice nucleation in MACM, though an explicit distribution of ice crystal number concentration is still calculated on the CRM grid. *Wang et al.* [2011b, 2012] found a weaker influence of aerosol on the shortwave cloud forcing than in CAM5, which is more consistent with observations and high-resolution models.

[19] In this experiment, MACM is configured following *Wang et al.* [2011a], with the outer GCM settings the same as CAM5 above and the inner CRM arranged in two dimensions with 32 vertical columns spaced at 4 km horizontal resolution. The CRM is a modified version of the System for Atmospheric Modeling, a detailed description of which is given by *Wang et al.* [2011a].

2.2. Nudging Description

[20] CAM5 has been modified to include nudging, a method for constraining a GCM's dynamical state by adding a forcing to the prognostic equations that relaxes the model toward prescribed atmospheric conditions. This forcing is given in equation (1), where X includes horizontal winds and dry static energy, X_M is the model calculated field, X_P is the prescribed field, τ is a relaxation time parameter, and ∂t is the model time step. In other words, the approach is a Newtonian relaxation technique, as used in early numerical forecast and data assimilation models [*Hoke and Anthes*, 1976]. It has since been put forth as an evaluation technique for GCMs [*Jeuken et al.*, 1996; *Machenhauer and Kirchner*, 2000], and has been used in chemical transport models [*Feichter and Lohmann*, 1999] and studies of the direct aerosol forcing [*Ghan et al.*, 2001] to constrain gas and particle plumes. Recent studies with the ECHAM5-HAM model have employed this technique to reduce differences in dust and sea salt emissions between simulations in order to test the sensitivity of aerosol indirect effects to varied model parameters [*Lohmann and Hoose*, 2009; *Lohmann and Ferrachat*, 2010]. *Jeuken et al.* [1996] describe the method in detail as well as the implications of adding unphysical terms to an already balanced physical model. The current implementation has been adapted from earlier versions of CAM used to initialize forecast simulations for evaluating the growth of model errors on short time scales [*Boyle et al.*, 2005]. Surface pressure nudging has not been included for CAM5 to be more consistent with conservation of mass assumptions used in the finite volume dynamical core.

$$\frac{\partial X_M}{\partial t} = \ldots - \frac{X_M - X_P}{\tau}. \quad (1)$$

[21] Nudging has typically been used to constrain model simulations to follow observed conditions, where X_P is obtained from analyzed observations. This approach has many benefits for comparing simulations to observed events and initializing realistic forecasts. However, in practice nudging toward conveniently gridded observations produced by reanalysis models can lead to unintended consequences due to systematic differences between the GCM and the reanalysis model, which in turn can affect parameterizations that may be tuned to compensate for inherent climatological model biases. *Lohmann and Hoose* [2009] note enhanced convection and precipitation in the tropics when ECHAM5-HAM is nudged toward European Centre for Medium-Range Weather Forecasts (ECMWF) ERA40 reanalysis. Similarly, the use of ECMWF ERA-Interim reanalysis [*Dee et al.*, 2011] as a nudging reference was explored during the early stages of this research, but this approach was found to introduce uncertainties in the comparison between aerosol indirect effects produced in free-running and nudged modes. For example, the global mean precipitation rate in free-running CAM5 simulations is 2.95 mm/day, but is reduced to 2.65 mm/day when nudging toward ERA-Interim reanalysis is included. While both of these values are realistically within the range of observational estimates, this result highlights the fact that nudging can have a significant impact on model physics and needs to be implemented carefully. Thus, instead of nudging toward ERA-Interim reanalysis, a

Table 1. Summary of Forcings for Each Simulation[a]

	PI (N)	PD (N)	PI (F)	PD (F)
Nudging	⇐ PI (F) ⇒		X	X
SSTs	⇐ 2000 (PD Climatology) ⇒			
GHGs	⇐ 2000 (PD Climatology) ⇒			
Aerosol	1850	2000	1850	2000

[a]All simulations used the same present-day (PD) climatological SSTs and GHGs representing the year 2000. Pre-industrial (PI) aerosol emissions are from the year 1850 and present-day are from the year 2000.

free-running simulation was first run for this experiment in order to generate a reference meteorology, which both pre-industrial and present-day simulations were then nudged toward. This procedure eliminated model-to-model differences and significantly reduced the impact of nudging on unconstrained fields, altering the global mean precipitation rate by less than 0.2%. Further details are discussed in the Experiment Design and Results and Discussion sections below.

[22] The value of the relaxation parameter (τ) determines how tightly the model is constrained to follow prescribed conditions and how much influence model physics are able to exert [*Jeuken et al.*, 1996]. The main criterion for the selection of this value for this research is the influence of nudging on relevant physical processes and its utility in isolating global aerosol indirect effects. With this consideration in mind, two relevant questions emerge: (1) on what timescale does the aerosol indirect effect stop being a radiative forcing and become a feedback? and (2) what is the relevant timescale for evaluating cloud-lifetime effects? A six-hour relaxation time was chosen, because it is longer than the lifetime of an individual cloud, so it does not dampen cloud-lifetime effects, but it also does not allow temperature perturbations and subsequent feedback responses persisting longer than six hours to influence the large-scale circulation. This choice is consistent with the assumption in CAM5 that unresolved clouds continuously dissipate and regenerate on a one-hour timescale [*Liu et al.*, 2012]. Future sensitivity experiments with other relaxation times and coupled ocean simulations may provide useful insight for discriminating the role of short-term feedbacks on aerosol-cloud effects versus longer-term effects linked to organized convection, but this topic is left for future research. The focus here is reducing natural variability differences between pre-industrial and present-day simulations, which introduce noise in the calculation of radiative forcing. Humidity is not nudged in this experiment, since the conversion of water vapor to liquid/ice is strongly mediated by the concentration and chemical makeup of ambient aerosol particles. Large-scale circulation, synoptic waves, and surface pressure are well constrained by nudging horizontal winds and dry static energy alone.

3. Experiment Design

[23] Results from four 10-year CAM5 simulations and four 1-year MACM simulations are evaluated in this study. Table 1 summarizes the external forcings for both the CAM5 and MACM sets of simulations. Two were conventional, unconstrained simulations (F - free-running) and two contained the nudging modifications described above (N - nudged). For both cases the model was run with annually repeating pre-industrial (PI – year 1850) and present-day (PD – year 2000) aerosol and precursor gas emissions created for IPCC AR5 experiments and described in *Neale et al.* [2010] and *Liu et al.* [2012]. All simulations were driven by annually repeating present-day Hadley Center sea surface temperatures/ice (monthly mean values representing the climatology for years 1981 to 2001 were interpolated to the model's time step) and present-day greenhouse gas concentrations (i.e., a fixed CO_2 surface concentration of 367 ppm) [*Neale et al.*, 2010]. For the nudged cases, six-hourly horizontal wind and dry static energy fields from the PI(F) simulation provided the prescribed atmospheric conditions, which were cubically interpolated internally to the model's time step and forced with a six-hour relaxation time.

[24] The first year of each CAM5 simulation was excluded from the results presented below, in order to allow aerosol and land surface fields to spin-up to climatological values. For MACM, five months of spin-up were used. Comparisons between the aerosol indirect effect (calculated here as the difference in cloud forcing between PI and PD simulations) in free-running and nudged modes on a variety of time scales demonstrate the role of nudging in suppressing natural variability and feedback responses to reduce noise and improve statistical significance. The aerosol indirect effect defined in this way represents the net effect of aerosol on cloud properties including both the albedo and lifetime effects, which differs from values reported in the IPCC AR4 that only included the albedo effect. To further demonstrate the utility of nudging for reducing the required simulation length, the free-running CAM5 simulations were extended for an additional ninety years, to provide a 100-year analysis for comparison with the 10-year results described above.

4. Results and Discussion

4.1. CAM5 Nudging Evaluation

[25] Nudging constrains specific meteorological fields, dry static energy and horizontal winds in the present research, to follow prescribed atmospheric conditions, reducing the average RMS errors shown in Table 2 (top) by 95%, 99%, and 98% for temperature, zonal, and meridional winds, respectively relative to the PI(F) simulation. However, since nudging is not a physically based forcing, it is also important to consider the impact it may have on unconstrained model fields.

[26] One potential concern is that the prescribed fields themselves already contain thermodynamic and dynamic responses to convective processes from the PI(F) simulation and might reduce the convective response required in the nudged simulation in order to remove an atmospheric instability. If this were the case, it would reduce the influence of model physics on the simulation result and the ability of physical parameterizations to respond to atmospheric and aerosol conditions. Nudging would play a dominant role and would mask the phenomena of interest, in this case the aerosol indirect effect. We can evaluate the importance of this potential concern after the fact, by analyzing the model tendencies.

[27] This concern does not appear to be a problem in this study, as can be seen in the global mean, column integrated temperature tendencies from dynamics, total physics, shallow/

Table 2. CAM5 Global-Annual Root Mean Square Error Relative to the Pre-industrial Free-Running Simulation and Mean Vertically Integrated Heating Tendencies (W/m^2)

	Root Mean Square Error		
	PD (F)	PD (N)	PI (N)
Temperature (K)	0.41	0.02	0.02
Zonal Wind (m/s)	1.07	0.01	0.01
Meridional Wind (m/s)	0.59	0.01	0.01
	Mean Vertically Integrated Heating Tendencies		
	PD (F)	PD (N)	N - F
Total Dynamics	−2.37	−2.42	−0.05
Total Physics	2.39	2.44	0.06
Shallow Convection	42.14	42.55	0.41
Deep Convection	41.87	41.84	−0.03
Radiation	−81.45	−81.30	0.14
Nudging	0.00	0.32	0.32

deep convention, radiation, and nudging given in Table 2 (bottom). The nudging tendency is small compared to that due to the physical parameterizations, and it changes the magnitude of other tendencies by less than 1%. Since nudging is included in the total physics tendency, the magnitude of the total physics tendency is slightly larger in the nudged simulations, by about 2.5%, a relatively small increase.

[28] Another potential concern is that unconstrained model fields may become more unrealistic in comparison to observations under nudging. This is especially true for nudging experiments that use reanalyzed observations as a reference atmospheric state, which can introduce additional model differences and biases. As noted earlier, the use of the ERA-Interim reanalysis as the reference data for nudging resulted in a reduction of the global mean precipitation rate by 10%. It also increased the liquid and ice water paths by 14% and 3%, respectively. In some ways, these changes led to model results that were in better agreement with observations, with two examples being reducing the double Inter Tropical Convergence Zone (ITCZ) problem and improving the position of Southern Hemisphere storm tracks. However, for the purposes of this study, these differences added uncertainty to the comparison between nudged and free-running simulations. The approach used here aimed to minimize all influences of nudging which are not essential to reducing natural variability differences between PI and PD simulations. In other words, the experimental design allows the model to behave much as it does in free-running mode, while constraining weather conditions (referred to here as "meteorology") consistently across the two simulations.

[29] Table 3 summarizes the effect of nudging on global-annual mean radiative and convective properties in the present climate. Global mean values, spatial root mean square errors, and pattern correlations shown in Table 3 are based on 10-year PD simulations and observations from 2001 to 2010 of top-of-atmosphere (TOA) radiative fluxes, cloud fraction, precipitable water, cloud water path, and precipitation. The inclusion of nudging led to a small decrease in the magnitude of shortwave cloud forcing, cloud fraction, cloud water path, and precipitation (0.60 W/m^2, 0.50%, 0.40 g/m^2, and 0.01 mm/day, respectively), and a small increase in the magnitude of outgoing clear-sky longwave radiation (0.20 W/m^2). Correlations between observations and the nudged simulation are nearly identical to those from the free-running simulation, and RMS errors are within 3%. The simulated outgoing all-sky shortwave (longwave) radiation and cloud-forcing were higher (lower) than observed. While both simulated shortwave and longwave clear-sky outgoing radiation were lower than observed. Lower cloud fraction in the nudged simulation was the result of a decrease in liquid water path from 48.4 g/m^2 in the free-running simulation to 47.6 g/m^2. Although the simulated total cloud water paths are low compared to NCEP CFSR (NOAA's National Centers for Environmental Prediction Climate Forecast System Reanalysis [*Saha et al.*, 2010]), there is a large range in estimates from satellite observations. Liquid water path from CERES (Clouds and the Earth's Radiant Energy System) Terra SYN1deg-lite_Ed2.6 data [*Wielicki et al.*, 1996] has a global mean value of 47.1 g/m^2 and recent analysis of CloudSat and MODIS observations give a range between 30 g/m^2 and 50 g/m^2 [*Jiang et al.*, 2012]. An evaluation of liquid and ice water paths in CAM5 and other IPCC AR5 models relative to satellite

Table 3. CAM5 Simulated and Observed Present-Day Global Mean, Spatial Root Mean Square Error, and Pattern Correlation Between Observations and Simulations

	Global Mean			RMSE		Correlation	
	OBS	PD (N)	PD (F)	PD (N)	PD (F)	PD (N)	PD (F)
Net All-sky[a] (W/m^2)	−339.4	−337	−337.4	11.5	11.7	0.9	0.9
SW All-sky[a] (W/m^2)	−99.7	−100.4	−101.0	14.0	14.0	0.8	0.8
LW All-sky[a] (W/m^2)	−239.8	−236.6	−236.4	7.7	8.0	1.0	1.0
Net Cloud-forcing[a] (W/m^2)	−21.1	−27.8	−28.4	13.5	14.2	0.7	0.7
SW Cloud-forcing[a] (W/m^2)	−47.3	−49.6	−50.2	15.0	15.2	0.8	0.8
LW Cloud-forcing[a] (W/m^2)	26.2	21.8	21.8	7.9	7.8	0.9	0.9
Net Clear-sky[a] (W/m^2)	−318.4	−309.2	309.1	10.6	10.8	1.0	1.0
SW Clear-sky[a] (W/m^2)	−52.4	−50.8	−50.8	5.7	5.8	1.0	1.0
LW Clear-sky[a] (W/m^2)	−266.0	−258.4	−258.2	8.4	8.6	1.0	1.0
Cloud fraction[b] (%)	61.3	62.1	62.6	10.2	10.1	0.8	0.8
Precipitable water[b] (kg/m^2)	24.3	25.8	25.8	2.4	2.4	1.0	1.0
Cloud water path[c] (g/m^2)	95.5	63.9	64.3	65.1	64.6	0.3	0.3
Precipitation[d] (mm/day)	2.68	2.95	2.95	1.08	1.10	0.9	0.9

[a]Observed TOA radiative fluxes are from CERES EBAF_Ed2.6 (Energy Balanced and Filled) for years 2001 to 2010 [*Loeb et al.*, 2009].
[b]Observed cloud fraction and precipitable water are from CERES Terra SYN1deg-lite_Ed2.6 for years 2001 to 2010 [*Wielicki et al.*, 1996].
[c]Observed cloud water path is from NCEP Climate Forecast System Reanalysis for years 2001 to 2010 [*Saha et al.*, 2010].
[d]Observed precipitation is from GPCP (Global Precipitation Climatology Project) for years 2001 to 2010 [*Adler et al.*, 2003].

Table 4. CAM5 Global Mean Aerosol Sources in Tg/yr (SO_4 in Tg S/yr), Sinks in Percent Dry (Wet) Deposition, and Burden (Lifetime) in Tg (SO_4 in Tg S) and Days

	PI (N)	PI (F)	PD (N)	PD (F)
		Sources in Tg/yr (SO_4 in Tg S/yr)		
Sulfate	15.69	15.85	49.76	50.15
Emission	0.38	0.38	1.66	1.66
Gas-phase	5.05	5.03	17.02	16.86
Aqueous-phase	10.26	10.44	31.08	31.63
Black Carbon	3.02	3.02	7.76	7.76
Primary Organic Matter	31.20	31.20	50.25	50.25
Secondary Organic Aerosol	91.51	91.51	102.19	102.19
Dust	3031.29	3061.59	2972.74	2928.25
Sea Salt	4749.19	4781.21	4749.57	4768.04
		Sinks in Percent Dry (Wet) Deposition		
Sulfate	12.5 (87.5)	12.3 (87.7)	12.8 (87.2)	12.8 (87.2)
Black Carbon	17.8 (82.2)	17.7 (82.3)	17.6 (82.4)	17.6 (82.4)
Primary Organic Matter	17.1 (82.9)	17.0 (83.0)	16.4 (83.6)	16.4 (83.6)
Secondary Organic Aerosol	10.9 (89.1)	10.8 (89.2)	12.5 (87.5)	12.7 (87.3)
Dust	64.1 (35.9)	63.9 (36.1)	64.7 (35.3)	64.3 (35.7)
Sea Salt	50.1 (49.9)	49.8 (50.2)	50.3 (49.7)	50.1 (49.9)
		Burden (Lifetime) in Tg (SO_4 in Tg S) and Days		
Sulfate	0.19 (4.4)	0.19 (4.4)	0.63 (4.6)	0.62 (4.5)
Black Carbon	0.04 (5.2)	0.04 (5.1)	0.10 (4.9)	0.10 (4.8)
Primary Organic Matter	0.45 (5.3)	0.45 (5.2)	0.75 (5.4)	0.74 (5.4)
Secondary Organic Aerosol	1.19 (4.8)	1.17 (4.6)	1.39 (5.0)	1.36 (4.9)
Dust	22.86 (2.8)	22.95 (2.7)	22.70 (2.8)	22.02 (2.7)
Sea Salt	11.46 (0.9)	11.23 (0.9)	11.61 (0.9)	11.32 (0.9)

observations is given by *Jiang et al.* [2012]. The spatial patterns of the resulting cloud fraction and precipitation fields are in good agreement with observations. However, some notable discrepancies include the double ITCZ, weaker (stronger) precipitation over South America (the Himalayas), and lower cloud fraction between Africa and Australia (not shown).

[30] In summary, the overall role of nudging improves the correlation between prescribed and modeled horizontal winds and temperature, constraining large-scale meteorology and circulation as intended. The above analysis demonstrates that this has been achieved without making unconstrained model fields any less realistic than free-running simulations within the uncertainty of observations.

4.2. CAM5 Aerosol Fields

[31] Since the purpose of this study is to assess the role of aerosol as a climate forcing agent, anthropogenic contributions to aerosol emissions and concentrations are summarized, and the impact of nudging on the mean aerosol burden is evaluated.

[32] Direct emission inventories represent the only sources for BC, POM, and SOA, which are identical for free-running and nudged simulations. SO_4^{2-} sources include both direct emissions from prescribed inventories and parameterized secondary production from SO_2 and DMS. Both dust and sea salt emissions are interactively calculated online, and are therefore affected by differences in natural variability as well as potential aerosol induced changes in surface wind speeds, precipitation/soil moisture, etc. Total sources shown in Table 4 (top) increased from PI to PD by 217/216% (N/F) for SO_4^{2-}, 157% for BC, 61% for POM, and 12% for SOA. Dust emissions were slightly reduced in the PD simulation by 2/4% (N/F), while changes in sea salt emissions were negligible. For SO_4^{2-}, direct emissions only contributed 2.4% (PI) and 3.3% (PD) to total sources, gas-phase production contributed 32.2/31.7% (PI, N/F) and 34.2/33.6% (PD, N/F), and aqueous production contributed 65.4/65.9% (PI, N/F) and 62.5/63.1% (PD, N/F). In the PD simulations, the magnitude of SO_4^{2-} production increased significantly, but the relative contribution from individual sources changed by less than 3%. Differences in the secondary production of SO_4^{2-} between nudged and free-running simulations are small and arise due to natural variability and a small reduction in cloud liquid water and therefore aqueous production in the nudged runs.

[33] Removal of aerosol particles from the atmosphere in CAM5 occurs through both wet and dry deposition, the combination of which is equal to total sources in the 10-year average, since aerosol lifetimes are on the order of days. The percentages of aerosol mass removed by dry and wet deposition separately are shown in Table 4 (middle). For SO_4^{2-}, BC, POM, and SOA, wet deposition is the dominant removal process and contributes over 80% in all simulations. Since most of the mass for dust and sea salt is contained in the coarse mode, dry deposition plays a more significant role, removing 64% and 50%, respectively. The relative contributions of dry and wet deposition to total removal changes little from PI to PD, less than 2% for all species. Differences between nudged and free-running simulations are less than 0.4%, indicating that removal processes important to aerosol are not affected by the inclusion of nudging.

[34] As expected, nudging did not strongly impact the effect of industrialization on mean aerosol burdens. Aerosol burdens and lifetimes resulting from the sources and sinks above are given in Table 4 (bottom) for both nudged and free-running simulations. Similar to production rates, aerosol burdens increased in the PD simulations by 232/226% (N/F)

for SO_4^{2-}, 150% for BC, 67/64% (N/F) for POM, and 17/16% (N/F) for SOA. Dust burdens decreased slightly in the PD simulation by 1/4% (N/F) and sea salt increased by 1%. Lifetimes increased by 0.1 to 0.3 days for SO_4^{2-}, POM, and SOA, decreased by 0.3 days for BC, and showed no change for dust and sea salt. Sea salt and dust have the largest burdens and shortest lifetimes because most of their total mass is in the coarse mode, which is removed quickly by dry deposition. In general, burdens and lifetimes are slightly smaller in the nudged simulations. However, these differences are small, less than 0.03 Tg (Tg S) for SO_4^{2-}, BC, POM, and SOA, less than 0.68 Tg for dust and sea salt, and less than 0.1 days for all lifetimes.

[35] The total global mean aerosol burden changed from PI to PD by 0.03 mg/m^2, 3.52/3.33 mg/m^2 (N/F), and $-0.12/-1.53$ mg/m^2 (N/F) for Aitken, accumulation, and coarse modes, respectively. The Aitken mode burden increased across the northern hemisphere, most significantly over China, the United States, and Europe. The accumulation mode burden increased over all landmasses and across northern hemisphere oceans. The coarse mode burden decreased slightly over northern Africa and Asia in association with decreased dust emissions in discrete regions. BC and POM contributed increased emissions and burden over Asia, central Africa, Amazonia, and eastern Europe, and decreased in the eastern United States. SO_4^{2-} sources and burden increased across the northern hemisphere, most significantly in the eastern United States, Europe, India, and China. SOA emissions increased over eastern North America, Europe, and parts of Asia. Regional changes in the sea salt burden in the free-running simulation were noisy, but the nudged simulation showed an increase over the northern hemisphere Pacific Ocean and along the western coast of subtropical landmasses.

[36] In summary, the effect of industrialization on aerosol burden in the nudged version of the model is quite comparable to the free-running version. The above analysis affirms the nudging technique as an appropriate tool to reduce internal variability in order to isolate aerosol indirect effects.

4.3. CAM5 Forcings and Indirect Effects

[37] Anthropogenic aerosol indirect effects, when treated as a quasi-forcing, are estimated as the difference in annual cloud forcing between simulations with pre-industrial and present-day aerosol emissions, in which both simulations have the same sea surface temperatures [*Rotstayn and Penner*, 2001]. Estimates of the shortwave contribution to the aerosol indirect effect from the 10-year nudged, 10-year free-running, and 100-year free-running simulations have global mean and 95% confidence interval values of -1.54 ± 0.02 W/m^2, -1.63 ± 0.17 W/m^2, and -1.61 ± 0.04 W/m^2, respectively. When longwave effects are also included, the mean net (shortwave plus longwave) flux change and 95% confidence interval values from the three simulations are -1.19 ± 0.02 W/m^2, -1.37 ± 0.13 W/m^2, and -1.35 ± 0.04 W/m^2, respectively. These values are about three times larger than clear-sky shortwave effects (direct aerosol effects and changes to the surface albedo), which have mean and 95% confidence interval values from the three simulations of -0.44 ± 0.01 W/m^2, -0.49 ± 0.05 W/m^2, and -0.48 ± 0.02 W/m^2, respectively. Nudging reduces the width of the net confidence interval by seven times relative to 10-year free-running simulations and by two times relative to 100-year free-running simulations.

[38] The net indirect effect from the 10-year nudged simulation is 0.16 W/m^2 smaller than the 100-year free-running simulation and is separated at 95% confidence intervals by 0.10 W/m^2. One interesting hypothesis for this statistically significant effect of nudging relates to the choice of a six-hour nudging timescale. It is plausible that since temperature perturbations in response to anthropogenic aerosol are dampened in the nudged simulations, these differences in mean quasi-forcing values may have been due to positive cloud feedbacks that enhance the forcing in free-running simulations on time scales longer than six hours. From this perspective, comparisons between free-running simulations, which include such feedbacks, and nudged simulations, which do not, may offer a useful method for isolating possible aerosol induced feedbacks. Additional experiments are encouraged to explore this hypothesis by examining the sensitivity of the nudged aerosol indirect effect across a range of relaxation timescales. We anticipate that such experiments may have the potential to help isolate the relevant time scales important to different components of the aerosol-cloud feedback processes.

[39] The statistics in Table 5 suggest that a single year of nudged integration can produce estimates of the aerosol indirect effect that are representative of a multidecadal free-running simulation. Global mean changes from PI to PD include changes in liquid/ice water path, column droplet/ice number concentration, and precipitation as well as radiative flux changes. For each field in Table 5 the global mean value, annual standard deviation, and pattern correlation is given for 10-year nudged, 10-year free-running, and 100-year free-running simulations. Annual standard deviations are reduced by 67% to nearly 100% with nudging. The pattern correlations for 10-year results compare estimates of the aerosol indirect effect between 1-year means and the 10-year mean, indicating how representative shorter time averages are of the long-term average. For 100-year results, the pattern correlation compares estimates of the aerosol indirect effect from 10-year means and the 100-year mean. In all cases, 1-year mean fields from the nudged simulations are more correlated (nearly double) with the 10-year mean than in the free-running simulations. Furthermore, 1-year mean correlations with the 10-year mean in the nudged simulations are higher than 10-year correlations with the 100-year mean in the free-running simulations. This indicates that the results obtained from 1-year simulations with nudging are likely to be more representative of the true mean than a set of 10-year free-running simulations.

[40] Figures 1 and 2 further demonstrate how constraining meteorology with nudging stabilizes estimates of the aerosol indirect effect. Figure 1 shows the spatial distribution of the net cloud forcing annual standard deviation from 10-year PD simulations and the difference between PI and PD simulations. Individual PD simulations have similar variability between run types, but the standard deviation of the difference between PI and PD is much lower for the nudged case. This is due to the fact that both the PI and PD simulations have the same circulation, and meteorology varies in the same manner. The global-annual net, shortwave, and longwave cloud forcing change from PI to PD for each simulated year shown in Figures 2a, 2b, and 2c are further evidence of

Table 5. CAM5 Global Mean, Annual Standard Deviation, and Pattern Correlation of the Difference Between Present-Day and Pre-industrial Simulations

	Global Mean			Standard Deviation			Correlation[a]		
	N-10	F-10	F-100	N-10	F-10	F-100	N-10	F-10	F-100
Net All-sky (W/m^2)	−1.54	−1.65	−1.69	0.02	0.19	0.24	0.96	0.62	0.91
SW All-sky (W/m^2)	−1.98	−2.13	−2.09	0.02	0.21	0.20	0.96	0.55	0.87
LW All-sky (W/m^2)	0.44	0.48	0.41	0.02	0.28	0.20	0.94	0.42	0.74
Net Cloud-forcing (W/m^2)	−1.19	−1.37	−1.35	0.02	0.18	0.2	0.95	0.59	0.89
SW Cloud-forcing (W/m^2)	−1.54	−1.63	−1.61	0.02	0.23	0.21	0.95	0.52	0.85
LW Cloud-forcing (W/m^2)	0.35	0.27	0.26	0.02	0.13	0.10	0.94	0.44	0.78
Net Clear-sky (W/m^2)	−0.36	−0.29	−0.33	0.01	0.19	0.16	0.91	0.46	0.7
SW Clear-sky (W/m^2)	−0.44	−0.49	−0.48	0.01	0.07	0.10	0.91	0.50	0.73
LW Clear-sky (W/m^2)	0.08	0.21	0.15	0.00	0.16	0.14	0.92	0.38	0.58
Liquid water path (g/m^2)	3.84	3.88	3.80	0.05	0.38	0.39	0.98	0.76	0.96
Column droplet # ($10^9/m^2$)	4.10	4.41	4.33	0.06	0.19	0.20	0.99	0.96	0.99
Ice water path (g/m^2)	0.10	−0.05	−0.07	0.01	0.13	0.16	0.89	0.40	0.76
Column ice # ($10^6/m^2$)	3.78	2.41	2.32	0.37	1.12	1.21	0.95	0.56	0.89
Precipitation (mm/day)	−0.01	−0.01	−0.01	0.00	0.01	0.01	0.92	0.37	0.67

[a]Pattern correlations for N-10 and F-10 compare 1-year means to the 10-year mean, F-100 compares 10-year means to the 100-year mean.

this. In the nudged case, each annual value falls close to the overall mean, while the difference between lowest and highest values is substantial in the free-running case (up to 0.80 W/m2 for the shortwave indirect effect). It is expected that, although the variability (standard deviation) does not decrease with simulation length, the standard error (annual standard deviation divided by the square root of the number of years) does, and the error in the free-running simulation should at some duration reduce to that of the nudged results. However, even after 100 years the standard error is still higher than the nudged results shown in Figure 2d.

[41] The 10-year simulated indirect effect described above resulted from a 38.7/40.6% (N/F) increase in column droplet number concentration, a 0.67 μm decrease in droplet mean radius, and a 3.84/3.88 g/m^2 (N/F) increase in liquid water path. Reduced droplet size and increased liquid water path contribute to higher cloud reflectivity and increase the average planetary albedo, reducing the amount of incoming solar radiation that reaches the surface. Consistent with a larger change in shortwave cloud forcing, the free-running PD simulation had a larger increase in droplet number concentration and liquid water path. Liquid water path, droplet number concentration, and droplet radius all showed similar patterns of change, most significantly over eastern Asia, off the northwest coast of South America, and across the northern Pacific Ocean, coincident with regions that showed

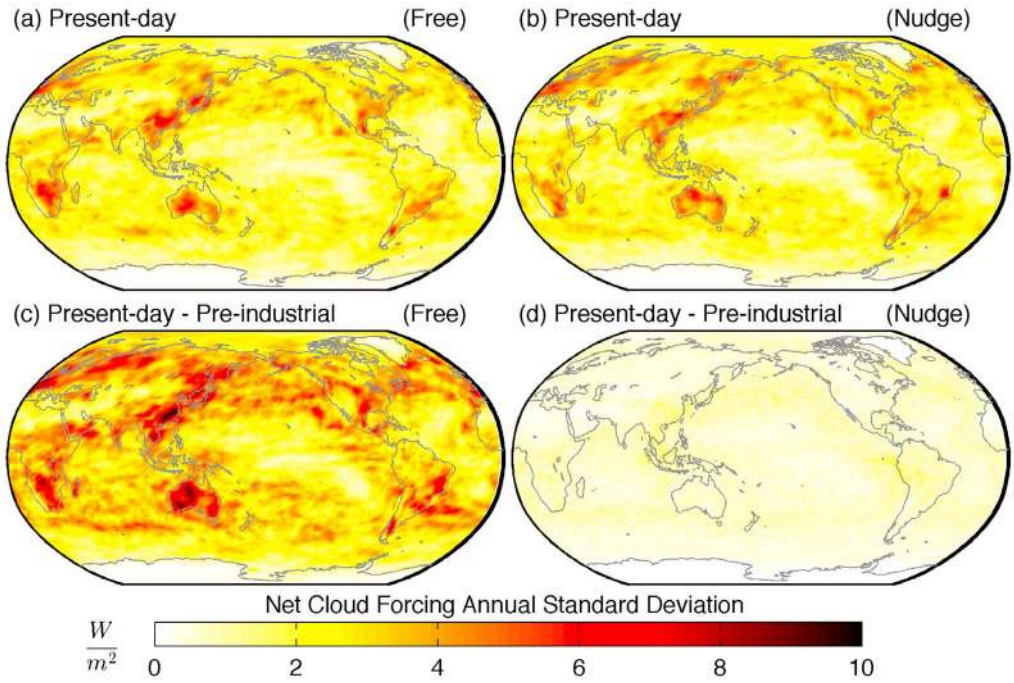

Figure 1. The standard deviation of the annual net cloud forcing from (a, b) individual present-day and (c, d) the difference between present-day and pre-industrial free-running (Figures 1a and 1c) and nudged (Figures 1b and 1d) CAM5 simulations.

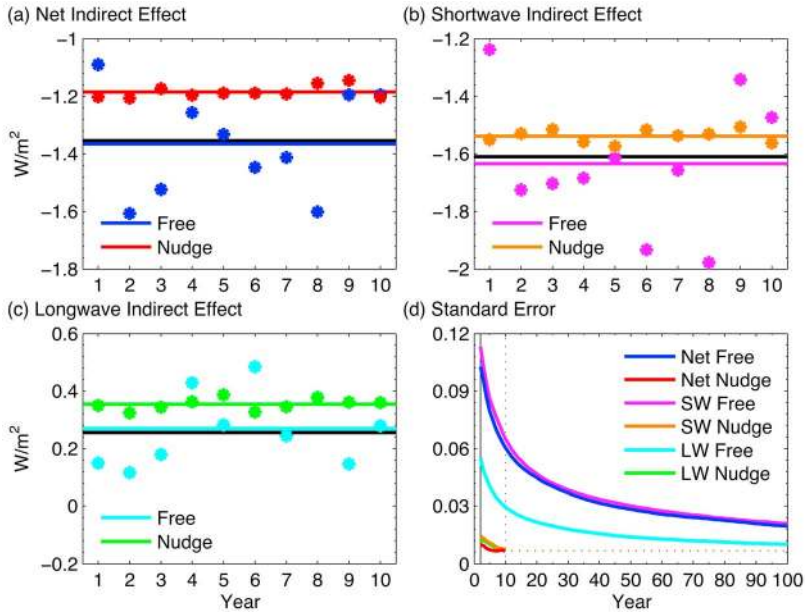

Figure 2. The global-annual mean (a) net, (b) shortwave, and (c) longwave cloud forcing difference between present-day and pre-industrial (aerosol indirect effect) in CAM5 for each simulation year and (d) the standard error as a function of the number of sample years. The solid lines in Figures 2a–2c indicate 10-year mean values and the black solid line indicates the 100-year mean value from the free-running simulation.

the largest decrease in shortwave cloud forcing (Figures 3c and 3d). Longwave radiation emission at the top of the atmosphere also increases with increased condensate, especially ice, which showed regional changes in patterns similar to longwave cloud forcing (Figures 3e and 3f). In general, changes in the longwave cloud forcing act to buffer the cooling pattern seen in the net aerosol indirect effect (Figures 3a and 3b), which is dominated by the shortwave forcing.

[42] It is clear from Figure 3 that the 10-year nudged results reproduce the signal from the 100-year free-running results and nudging achieves higher statistical significance in a tenth of the simulation length. Figure 4 demonstrates this further, showing the net aerosol indirect effect averaged for the first 3 years and 10 years of the simulations. Stippling indicates where the signal is significant at the 95% confidence interval for the given number of years. The 3-year free-running result has low statistical significance, but with nudging, three years is long enough to evaluate the spatial pattern of the signal where aerosol indirect effects are large. The 10-year free-running result begins to converge toward the nudged result, with less noise, and greater significance over Asia, the north Pacific, and off the northwest coast of South America. However, the 10-year nudged result is significant over a much wider area (66% versus 28% of the Earth's area), including almost the entire Northern Hemisphere.

[43] Overall, these results demonstrate that constraining simulations through the use of nudging provides a more stable global estimate of the aerosol indirect radiative forcing on short time scales and increases the regional statistical significance of the signal.

4.4. MACM Results

[44] Although MACM simulations can be scaled more efficiently on a much higher number of processors than CAM5, they require two hundred times more computational resources for a given amount of simulated time and therefore can currently be run for only a limited number of years. The above analysis of CAM5 has demonstrated that a one-year nudged simulation is highly correlated with the long-term average. Hence, one-year MACM simulations are analyzed in this study.

[45] Table 6 summarizes the differences between MACM in nudged and free-running modes and how each compares to observations. As was the case with CAM5, the addition of nudging has little impact on global mean radiative fields and cloud properties. Pattern correlations are identical for both run types, and the spatial RMS errors vary by less than 4%. With the exception of all-sky longwave, radiative flux errors are slightly smaller in MACM than CAM5. Cloud water path errors are also smaller, but cloud fraction, precipitable water, and precipitation errors are slightly higher. The only global mean values that differ by more than 4% between MACM and CAM5 are longwave cloud forcing and total cloud fraction. The global mean longwave cloud forcing in MACM is 18% higher than in CAM5 and is closer to CERES observations, although the pattern correlation is lower. The total cloud fraction is 6–7% lower in MACM than both CAM5 and CERES observations. These results are consistent with the MACM and CAM5 differences discussed and evaluated in detail by *Wang et al.* [2011a, 2011b].

[46] Results from 3-year free-running MACM simulations published by *Wang et al.* [2011b] are included as a baseline for comparison to the 1-year global mean values presented in

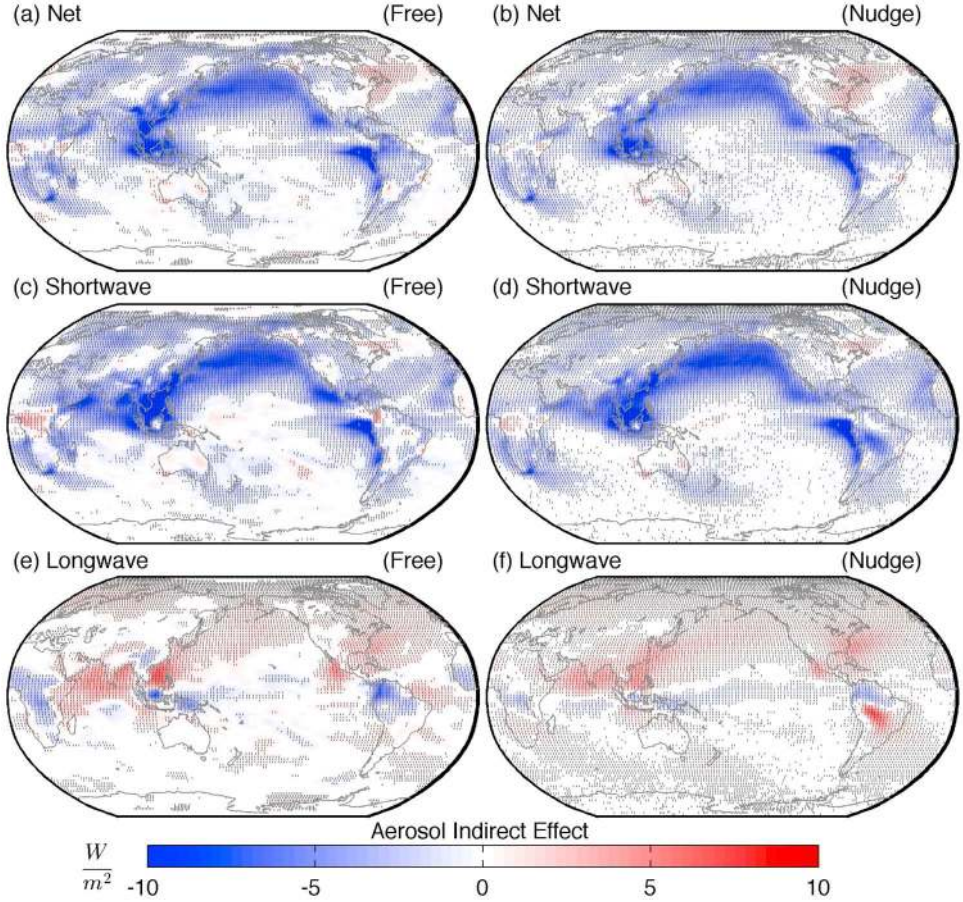

Figure 3. The (a, b) net, (c, d) shortwave, and (e, f) longwave cloud forcing difference between present-day and pre-industrial (aerosol indirect effect) in CAM5 100-year free-running (Figures 3a, 3c, and 3e) and 10-year nudged (Figures 3b, 3d, and 3f) simulations; stippling indicates where the signal is significant at the 95% confidence interval.

Table 7 from the present study. For almost all fields, the 1-year nudged results are in better agreement with those of *Wang et al.* [2011b] than the 1-year free-running results. In response to industrial aerosol loading, MACM produces a weaker change in the cloud forcing and a larger change in the clear-sky forcing than CAM5. The global mean shortwave cloud forcing in MACM is about half that of CAM5 with values of -0.80 W/m^2 and -0.56 W/m^2 for nudged and free-running, respectively. Changes in the longwave cloud forcing are even smaller, contributing to a net aerosol indirect effect of -0.81 W/m^2 and -0.82 W/m^2 for nudged and free-running simulations, respectively. Weaker indirect effects due to embedded explicit convection are consistent with those of *Wang et al.* [2011b, 2012] and result from a smaller increase in liquid water path of 4% and droplet number concentration of 25% in MACM compared to CAM5 values of 9% and 39/41% (N/F), respectively. Lower estimates of aerosol indirect effects such as these are also reported in GCM simulations in which aerosol-cloud relationships are constrained by satellite observations [e.g., *Dufresne et al.*, 2005].

[47] Two main factors account for the smaller changes in MACM: (1) LWP is less sensitive to CCN perturbations in MACM than CAM5 and (2) MACM has a smaller aerosol burden (and therefore CCN) perturbation with present-day emissions than CAM5, even though aerosol emissions are identical. *Wang et al.* [2011b] found that LWP increases by almost three times as much in CAM5 than MACM for a given change in CCN. *Wang et al.* [2012] linked this difference in LWP response to the representation of cloud lifetime effects using a new method for evaluating the impact of aerosol on precipitation called precipitation frequency susceptibility. They found that the smaller LWP response to aerosol perturbation in MACM can be explained by the smaller precipitation frequency susceptibility, which agrees better with satellite observations. Higher sensitivity in CAM5 results in greater changes to cloud properties that have a positive feedback on the production and removal rates of aerosol (e.g., cloud lifetime and precipitation rate) [*Wang et al.*, 2011b]. As a result, SO_4^{2-}, BC, POM, and SOA burdens in this study are 114/106% (N/F), 17%, 14/11% (N/F), 2/3% (N/F) higher in CAM5 than MACM, respectively. Future work will further investigate the mechanisms responsible for these differences, which will be more easily diagnosed with the reduction in noise from natural variability gained by nudging.

[48] In MACM, the impact that nudging has on global mean shortwave aerosol indirect effects appear to be opposite to that of CAM5; the shortwave effects from the nudged simulations are larger than those from both the 1-year and

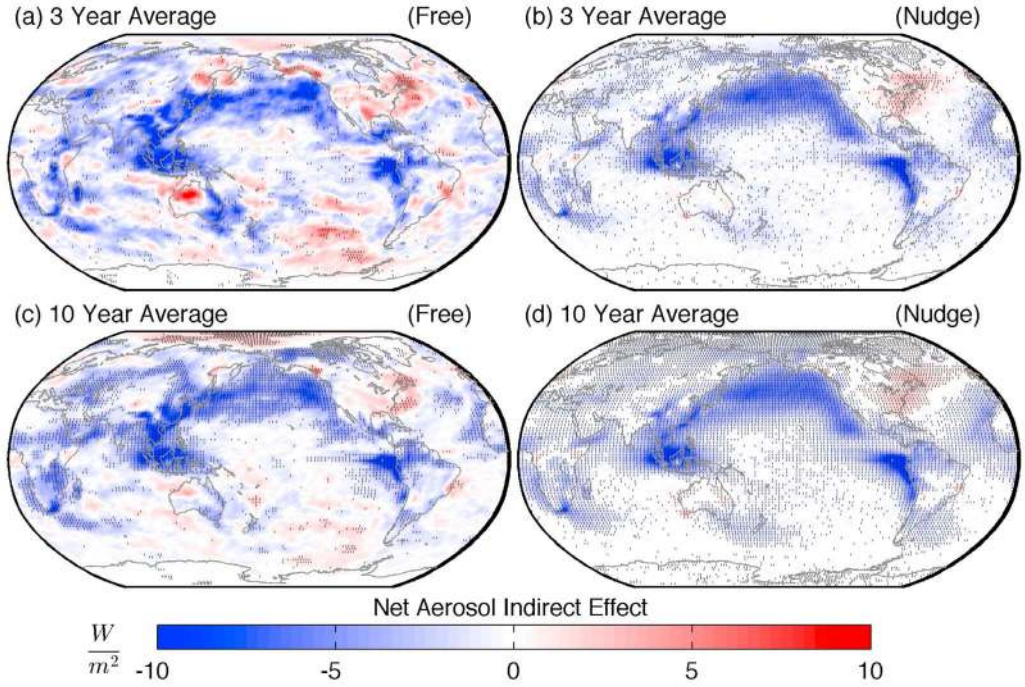

Figure 4. The net cloud forcing difference between present-day and pre-industrial (aerosol indirect effect) in CAM5 averaged for the first (a, b) 3 years and (c, d) 10 years of free-running (Figures 4a and 4c) and nudged (Figures 4b and 4d) simulations; stippling indicates where the signal is significant at the 95% confidence interval.

3-year free-running simulations. The most likely reason for this is that 3-year free-running simulations under-sample the variability of the aerosol forcing (which is also the likely reason for differences in the net TOA radiation between nudged and free-running simulations shown in Table 7). As shown in the CAM5 results from 10-year simulations, the range in variability of shortwave indirect effects from one year to another can be up to 0.8 W/m^2. However, it is also possible that MACM simulates negative shortwave cloud feedbacks in response to the aerosol forcing, and these are damped by the inclusion of temperature nudging. Further investigation of aerosol-induced feedback mechanisms and their representation in MACM is needed to determine which explanation is correct.

[49] Although the global mean aerosol indirect effect is quantitatively smaller in MACM, the spatial distribution shows a similar pattern to that of CAM5. The one-year mean net cloud forcing difference from PI to PD for CAM5 (first year) and MACM simulations are shown in Figures 5a–5d. Due to the noisiness of the free-running results, it is not possible to evaluate the regional structure of the forcing in a one-year simulation. However, in the nudged results from both models, the strongest signal occurs over the Northern Hemisphere Pacific Ocean and off the northwest coast of South America, where maxima in low-level clouds and shortwave cloud forcing are coincident with high anthropogenic aerosol burdens. Differences in the regional patterns between MACM and CAM5 can more clearly be evaluated

Table 6. Same as Table 3, Except for MACM

	Global Mean			RMSE		Correlation	
	OBS	PD (N)	PD (F)	PD (N)	PD (F)	PD (N)	PD (F)
Net All-sky (W/m^2)	−339.4	−336.3	−336.5	11.4	11.3	0.9	0.9
SW All-sky (W/m^2)	−99.7	−101.7	−101.9	13.2	13.3	0.7	0.7
LW All-sky (W/m^2)	−239.8	−234.6	−234.6	10.4	10.3	1.0	1.0
Net Cloud-forcing (W/m^2)	−21.1	−24.4	−24.6	11.5	11.7	0.7	0.7
SW Cloud-forcing (W/m^2)	−47.3	−50.2	−50.4	13.0	13.3	0.8	0.8
LW Cloud-forcing (W/m^2)	26.2	25.8	25.9	7.6	7.6	0.8	0.8
Net Clear-sky (W/m^2)	−318.4	−311.8	−312	8.5	8.5	1.0	1.0
SW Clear-sky (W/m^2)	−52.4	−51.5	−51.5	5.6	5.6	1.0	1.0
LW Clear-sky (W/m^2)	−266.0	−260.3	−260.5	6.7	6.7	1.0	1.0
Cloud fraction (%)	61.3	55.5	55.6	12.4	12.6	0.8	0.8
Precipitable water (kg/m^2)	24.3	25.5	25.5	2.6	2.7	1.0	1.0
Cloud water path (g/m^2)	95.5	65.5	65.9	52.3	52.1	0.5	0.5
Precipitation (mm/day)	2.68	2.84	2.85	1.23	1.24	0.8	0.8

Table 7. Same as Table 5, Except for MACM

	N	F	W[a]
Net All-sky (W/m^2)	−1.27	−1.52	−1.05
SW All-sky (W/m^2)	−1.37	−1.22	−1.31
LW All-sky (W/m^2)	0.10	−0.31	0.26
Net Cloud-forcing (W/m^2)	−0.81	−0.82	−0.83
SW Cloud-forcing (W/m^2)	−0.80	−0.56	−0.77
LW Cloud-forcing (W/m^2)	−0.01	−0.27	−0.06
Net Clear-sky (W/m^2)	−0.46	−0.7	−0.23
SW Clear-sky (W/m^2)	−0.57	−0.66	−0.54
LW Clear-sky (W/m^2)	0.11	−0.04	0.31
Liquid water path (g/m^2)	2.12	2.16	2.11
Column droplet # (10^9/m^2)	4.58	4.53	4.80
Ice water path (g/m^2)	−0.03	−0.10	0.00
Column ice # (10^6/m^2)	−1.58	−5.38	−2.00
Precipitation (mm/day)	−0.01	0.00	−0.01

[a]W refers to values from *Wang et al.* [2011b].

in the nudged simulation (Figure 5f), which is not possible without nudging due to significant noise in the 1-year free-running simulation (Figure 5e). The largest regional differences between MACM and CAM5 are a weaker forcing over SE Asia and off the northwest coast of South America and the absence of the positive forcing off the eastern coast of North America in the MACM simulations. These net differences are dominated by the pattern of change in shortwave cloud forcing (Figure 6e) and are consistent with MACM's lower sensitivity to large aerosol perturbations. Since the representation of ice nucleation in MACM does not depend on aerosol particle concentrations, the longwave aerosol indirect effect is much smaller than in CAM5 (Figure 6f).

5. Conclusions

[50] In this study, nudging has been implemented to constrain simulations with pre-industrial and present-day aerosol emissions toward identical circulation and meteorology. This method effectively reduces differences in natural variability and dampens feedback responses, to isolate radiative forcing. The global-annual mean net aerosol indirect radiative forcing is estimated to be −1.19, −1.37, and −1.35 W/m^2 in 10-year nudged, 10-year free-running, and 100-year free-running CAM5 simulations, respectively. A more stable global estimate of the aerosol indirect effect on short time scales is obtained with nudging, which increases the pattern correlation between 1-year and 10-year averages from 0.59 to 0.95. The area of the Earth that has a statistically significant aerosol indirect forcing signal at the 95%

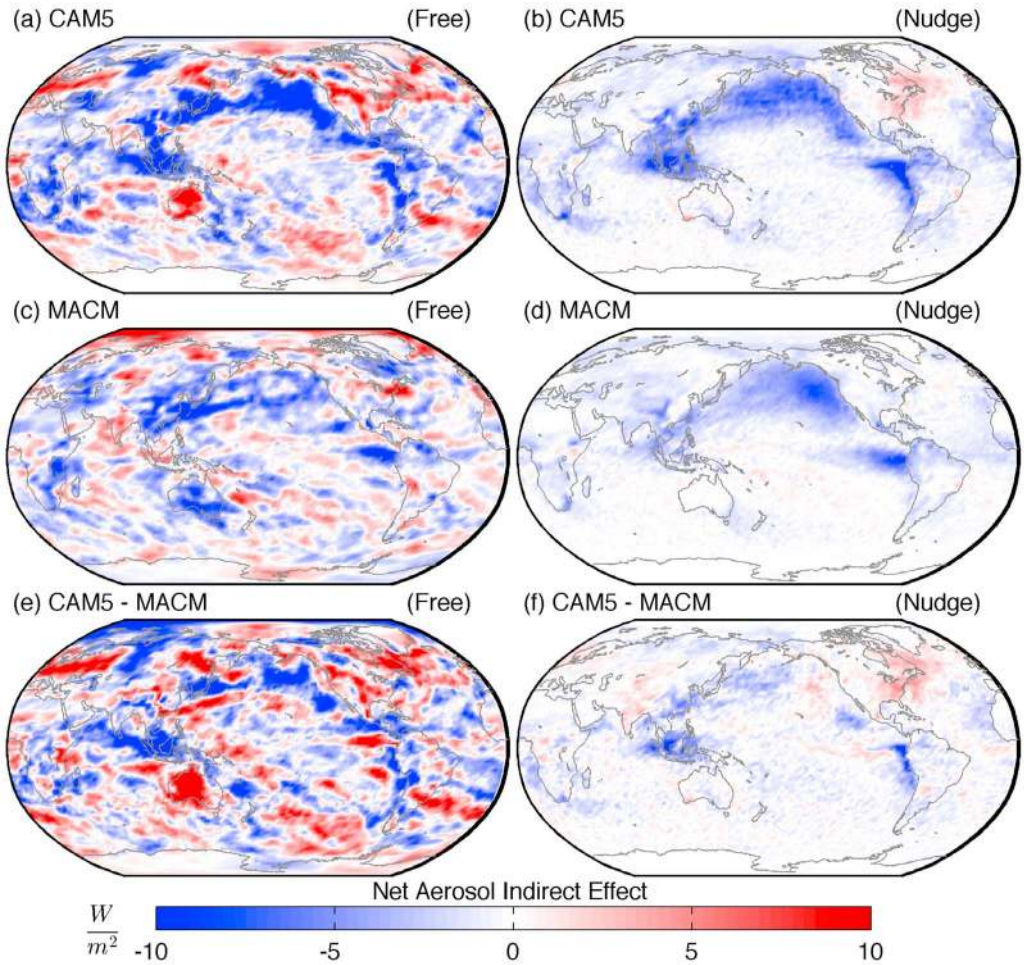

Figure 5. The net cloud forcing difference between present-day and pre-industrial (aerosol indirect effect) in (a, b) CAM5 (first year), (c, d) MACM, and (e, f) the difference between CAM5 and MACM free-running (Figures 5a, 5c, and 5e) and nudged (Figures 5b, 5d, and 5f) simulations.

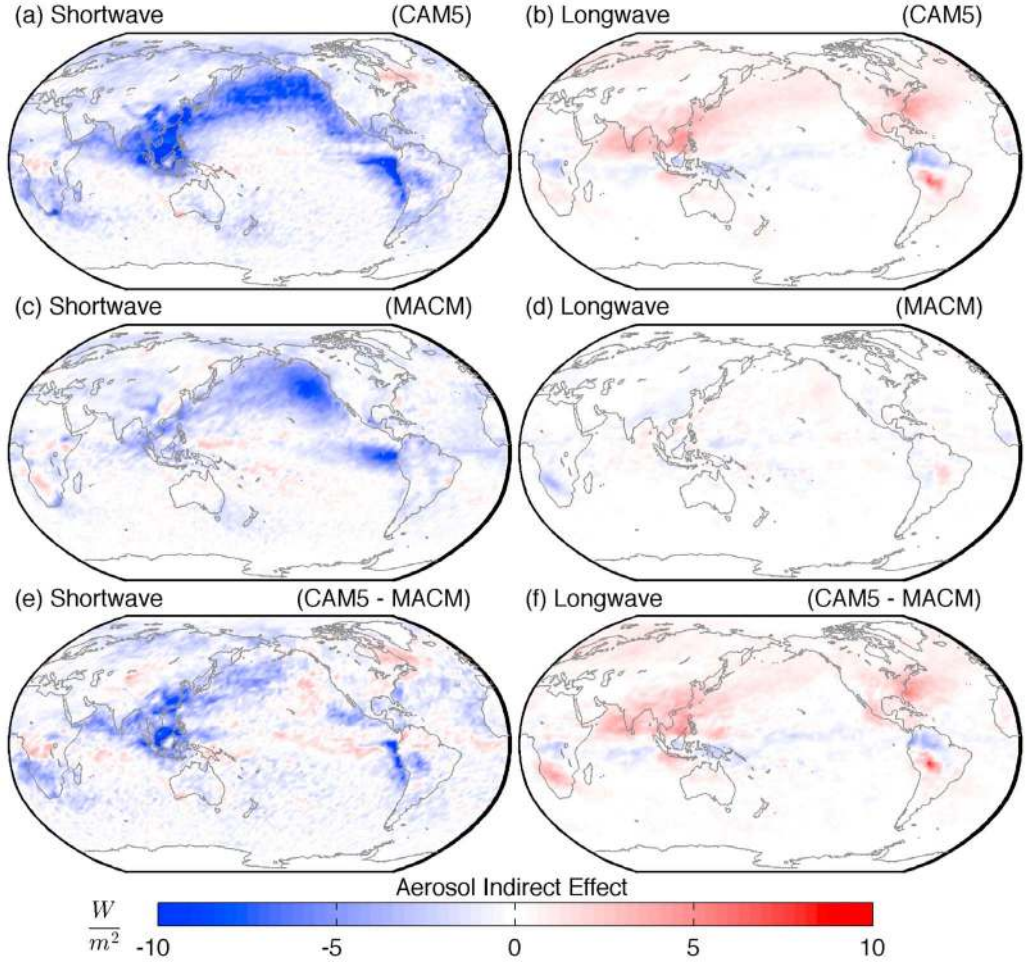

Figure 6. The (a, c, e) shortwave and (b, d, f) longwave cloud forcing difference between present-day and pre-industrial (aerosol indirect effect) in CAM5 (first year) (Figures 6a and 6b), MACM (Figures 6c and 6d), and the difference between CAM5 and MACM (Figures 6e and 6f) nudged simulations.

confidence interval is increased from 28% in the 10-year free-running simulations to 66% in the nudged simulations.

[51] A beneficial consequence of reducing differences in natural variability is that it also reduces the required simulation duration for estimating aerosol indirect effects, enabling computationally expensive next-generation aerosol-climate models to be brought to bear on the problem. MACM, a new Multiscale Aerosol Climate Model, simulated a smaller aerosol indirect effect than CAM5, with 1-year global mean values of -0.81 and -0.82 W/m^2 for nudged and free-running, respectively. The MACM value is significantly lower than the value from CAM5, which results from both smaller changes in the aerosol burden and a weaker relationship between CCN and LWP. The regional patterns of the aerosol indirect forcing in 1-year MACM and CAM5 free-running simulations are too noisy to evaluate. However, a clear increase in the magnitude of the net/shortwave cloud forcing in PD simulations can be seen across the North Pacific Ocean and near the northwestern coast of South America in the nudged simulations. A larger forcing in CAM5 relative to MACM is coincident with regions of the highest aerosol burdens (not shown).

[52] The fact that one-year nudged simulations show such a clear signal and are strongly correlated with longer time averages opens the opportunity for many future studies. The nudging approach presented here may be useful for isolating aerosol feedback responses on a variety of time scales, evaluating the regional structure of indirect effects in MACM and other computationally expensive models that explicitly resolve clouds, and comparing model simulations directly to field campaigns and satellite measurements by nudging toward reanalyzed observations.

[53] **Acknowledgments.** This research was supported by the Center for Multiscale Modeling of Atmospheric Processes (CMMAP), a National Science Foundation (NSF) Science and Technology Center managed by Colorado State University under Cooperative Agreement ATM-0425247. CMMAP funding for this study was provided through sub-awards to Richard Somerville and John Helly. This research was also supported in part by the U.S. Department of Energy's (DOE) Office of Science, Office of Biological and Environmental Research (BER) program under grant DE-SC0002003. Michael Pritchard acknowledges further support from the NOAA Climate and Global Change Postdoctoral Fellowship program. Steven Ghan and Minghuai Wang were supported by the DOE Office of Science, Decadal and Regional Climate Prediction using Earth System Models (EaSM) program. The Pacific Northwest National Laboratory (PNNL) is operated for the DOE by Battelle Memorial Institute under contract DE-AC06-76RLO 1830. The NSF XSEDE provided computing resources on the University of Tennessee's Kraken and Purdue University's Steele supercomputers under allocation numbers TG-ATM090002 and TG-ATM100027. CESM (CAM5) development was led by the National Center for Atmospheric Research (NCAR) and is supported by the NSF

and the DOE's Office of Science (BER). MACM was developed at the DOE's Pacific Northwest National Laboratory and the authors are grateful to Mikhail Ovchinnikov for valuable support and insight. We also thank Marat Khairoutdinov for originally implementing the MMF in CAM as well as for his and Jerry Olson's help with meteorologically constraining (nudging) the models. CERES data were obtained from the NASA Langley Research Center CERES ordering tool at (http://ceres.larc.nasa.gov/). CFSR and ERA-Interim data are from the Research Data Archive (RDA), which is maintained by the Computational and Information Systems Laboratory (CISL) at the NCAR and are available from the RDA (http://rda.ucar.edu/) in data set numbers ds093.2 (CFSR) and ds627.0 (ERA-Interim). GPCP Precipitation data were provided by the NOAA/OAR/ESRL PSD, Boulder, Colorado, USA, from their Web site at (http://www.esrl.noaa.gov/psd/). The authors would also like to thank the three anonymous reviewers for their thoughtful comments and suggestions.

References

Abdul-Razzak, H., and S. J. Ghan (2000), A parameterization of aerosol activation: 2. Multiple aerosol types, *J. Geophys. Res.*, *105*(D5), 6837–6844, doi:10.1029/1999JD901161.

Adler, R. F., et al. (2003), The Version 2 Global Precipitation Climatology Project (GPCP) Monthly Precipitation Analysis (1979-present), *J. Hydrometeorol.*, *4*, 1147–1167, doi:10.1175/1525-7541(2003)004<1147:TVGPCP>2.0.CO;2.

Albrecht, B. A. (1989), Aerosols, cloud microphysics, and fractional cloudiness, *Science*, *245*(4923), 1227–1230, doi:10.1126/science.245.4923.1227.

Andreae, M. O., D. Rosenfeld, P. Artaxo, A. A. Costa, G. P. Frank, K. M. Longo, and M. A. F. Silva-Dias (2004), Smoking rain clouds over the Amazon, *Science*, *303*(5662), 1337–1342, doi:10.1126/science.1092779.

Benedict, J. J., and D. A. Randall (2009), Structure of the Madden–Julian Oscillation in the superparameterized CAM, *J. Atmos. Sci.*, *66*(11), 3277–3296, doi:10.1175/2009JAS3030.1.

Bony, S., et al. (2006), How well do we understand and evaluate climate change feedback processes?, *J. Clim.*, *19*(15), 3445–3482, doi:10.1175/JCLI3819.1.

Boyle, J. S., D. Williamson, R. Cederwall, M. Fiorino, J. Hnilo, J. Olson, T. Phillips, G. Potter, and S. Xie (2005), Diagnosis of community atmospheric model 2 (CAM2) in numerical weather forecast configuration at Atmospheric Radiation Measurement sites, *J. Geophys. Res.*, *110*, D15S15, doi:10.1029/2004JD005042.

Bréon, F. M., D. Tanre, and S. Generoso (2002), Aerosol effect on cloud droplet size monitored from satellite, *Science*, *295*(5556), 834–838, doi:10.1126/science.1066434.

Coakley, J. A., R. L. Bernstein, and P. A. Durkee (1987), Effect of ship-stack effluents on cloud reflectivity, *Science*, *237*(4818), 1020–1022, doi:10.1126/science.237.4818.1020.

Dee, D. P., et al. (2011), The ERA-Interim reanalysis: Configuration and performance of the data assimilation system, *Q. J. R. Meteorol. Soc.*, *137*(656), 553–597, doi:10.1002/qj.828.

DeMott, P. J., K. Sassen, M. R. Poellot, D. Baumgardner, D. C. Rogers, S. D. Brooks, A. J. Prenni, and S. M. Kreidenweis (2003), African dust aerosols as atmospheric ice nuclei, *Geophys. Res. Lett.*, *30*(14), 1732, doi:10.1029/2003GL017410.

Dufresne, J.-L., J. Quaas, O. Boucher, S. Denvil, and L. Fairhead (2005), Contrasts in the effects on climate of anthropogenic sulfate aerosols between the 20th and the 21st century, *Geophys. Res. Lett.*, *32*, L21703, doi:10.1029/2005GL023619.

Easter, R. C., S. J. Ghan, Y. Zhang, R. D. Saylor, E. G. Chapman, N. S. Laulainen, H. Abdul-Razzak, L. R. Leung, X. D. Bian, and R. A. Zaveri (2004), MIRAGE: Model description and evaluation of aerosols and trace gases, *J. Geophys. Res.*, *109*, D20210, doi:10.1029/2004JD004571.

Feichter, J., and U. Lohmann (1999), Can a relaxation technique be used to validate clouds and sulphur species in a GCM?, *Q. J. R. Meteorol. Soc.*, *125*(556), 1277–1294.

Forster, P. M. F., and K. E. Taylor (2006), Climate forcings and climate sensitivities diagnosed from coupled climate model integrations, *J. Clim.*, *19*(23), 6181–6194, doi:10.1175/JCLI3974.1.

Forster, P. M. F., R. S. Freckleton, and K. P. Shine (1997), On aspects of the concept of radiative forcing, *Clim. Dyn.*, *13*, 547–560, doi:10.1007/s003820050182.

Forster, P., et al. (2007), Changes in atmospheric constituents and in radiative forcing, in *Climate Change 2007: The Physical Science Basis. Contribution of Working Group I to the Fourth Assessment Report of the Intergovernmental Panel on Climate Change*, edited by S. Solomon et al., pp. 129–234, Cambridge Univ. Press, Cambridge, UK.

Ghan, S. J., and R. C. Easter (2006), Impact of cloud-borne aerosol representation on aerosol direct and indirect effects, *Atmos. Chem. Phys.*, *6*(12), 4163–4174, doi:10.5194/acp-6-4163-2006.

Ghan, S., N. Laulainen, R. Easter, R. Wagener, S. Nemesure, E. Chapman, Y. Zhang, and R. Leung (2001), Evaluation of aerosol direct radiative forcing in MIRAGE, *J. Geophys. Res.*, *106*(D6), 5295–5316, doi:10.1029/2000JD900502.

Ghan, S. J., X. Liu, R. C. Easter, R. Zaveri, P. J. Rasch, J.-H. Yoon, and B. Eaton (2012), Toward a minimal representation of aerosols in climate models: Comparative decomposition of aerosol direct, semi-direct and indirect radiative forcing, *J. Clim.*, *25*, 6461–6476, doi:10.1175/JCLI-D-11-00650.1.

Gong, S. L., X. Y. Zhang, T. L. Zhao, X. B. Zhang, L. A. Barrie, I. G. McKendry, and C. S. Zhao (2006), A simulated climatology of Asian dust aerosol and its trans-Pacific transport. Part II: Interannual variability and climate connections, *J. Clim.*, *19*(1), 104–122, doi:10.1175/JCLI3606.1.

Grabowski, W. W. (2001), Coupling cloud processes with the large-scale dynamics using the Cloud-Resolving Convection Parameterization (CRCP), *J. Atmos. Sci.*, *58*(9), 978–997, doi:10.1175/1520-0469(2001)058<0978:CCPWTL>2.0.CO;2.

Grabowski, W. W., and P. K. Smolarkiewicz (1999), CRCP: A Cloud Resolving Convection Parameterization for modeling the tropical convecting atmosphere, *Physica D*, *133*(1–4), 171–178, doi:10.1016/S0167-2789(99)00104-9.

Gustafson, W. I., Jr., L. K. Berg, R. C. Easter, and S. J. Ghan (2008), The Explicit-Cloud Parameterized-Pollutant hybrid approach for aerosol-cloud interactions in multiscale modeling framework models: Tracer transport results, *Environ. Res. Lett.*, *3*, 025005, doi:10.1088/1748-9326/3/2/025005.

Hoke, J. E., and R. A. Anthes (1976), Initialization of numerical models by a dynamic initialization technique, *Mon. Weather Rev.*, *104*, 1551–1556, doi:10.1175/1520-0493(1976)104<1551:TIONMB>2.0.CO;2.

Jeuken, A. B. M., P. C. Siegmund, L. C. Heijboer, J. Feichter, and L. Bengtsson (1996), On the potential of assimilating meteorological analyses in a global climate model for the purpose of model validation, *J. Geophys. Res.*, *101*(D12), 16,939–16,950, doi:10.1029/96JD01218.

Jiang, J. H., et al. (2012), Evaluation of cloud and water vapor simulations in CMIP5 climate models using NASA "A-Train" satellite observations, *J. Geophys. Res.*, *117*, D14105, doi:10.1029/2011JD017237.

Kaufman, Y. J., I. Koren, L. A. Remer, D. Rosenfeld, and Y. Rudich (2005), The effect of smoke, dust, and pollution aerosol on shallow cloud development over the Atlantic Ocean, *Proc. Natl. Acad. Sci. U. S. A.*, *102*(32), 11,207–11,212, doi:10.1073/pnas.0505191102.

Khairoutdinov, M. F., and D. A. Randall (2001), A cloud resolving model as a cloud parameterization in the NCAR Community Climate System Model: Preliminary results, *Geophys. Res. Lett.*, *28*(18), 3617–3620, doi:10.1029/2001GL013552.

Khairoutdinov, M., D. Randall, and C. DeMott (2005), Simulations of the atmospheric general circulation using a cloud-resolving model as a superparameterization of physical processes, *J. Atmos. Sci.*, *62*(7), 2136–2154, doi:10.1175/JAS3453.1.

Köhler, H. (1936), The nucleus in and the growth of hygroscopic droplets, *Trans. Faraday Soc.*, *32*(2), 1152–1161, doi:10.1039/tf9363201152.

Leaitch, W. R., G. A. Isaac, J. W. Strapp, C. M. Banic, and H. A. Wiebe (1992), The relationship between cloud droplet number concentrations and anthropogenic pollution: Observations and climatic implications, *J. Geophys. Res.*, *97*(D2), 2463–2474, doi:10.1029/91JD02739.

Liu, X., and J. E. Penner (2005), Ice nucleation parameterization for global models, *Meteorol. Z.*, *14*(4), 499–514, doi:10.1127/0941-2948/2005/0059.

Liu, X., J. E. Penner, S. J. Ghan, and M. Wang (2007), Inclusion of ice microphysics in the NCAR Community Atmospheric Model Version 3 (CAM3), *J. Clim.*, *20*(18), 4526–4547, doi:10.1175/JCLI4264.1.

Liu, X., et al. (2012), Toward a minimal representation of aerosols in climate models: Description and evaluation in the Community Atmosphere Model CAM5, *Geosci. Model Dev.*, *5*(3), 709–739, doi:10.5194/gmd-5-709-2012.

Loeb, N. G., B. A. Wielicki, D. R. Doelling, G. L. Smith, D. F. Keyes, S. Kato, N. Manlo-Smith, and T. Wong (2009), Toward optimal closure of the Earth's TOA radiation budget, *J. Clim.*, *22*, 748–766, doi:10.1175/2008JCLI2637.1.

Lohmann, U., and J. Feichter (2005), Global indirect aerosol effects: A review, *Atmos. Chem. Phys.*, *5*, 715–737, doi:10.5194/acp-5-715-2005.

Lohmann, U., and S. Ferrachat (2010), Impact of parametric uncertainties on the present-day climate and on the anthropogenic aerosol effect, *Atmos. Chem. Phys.*, *10*, 11,373–11,383, doi:10.5194/acp-10-11373-2010.

Lohmann, U., and C. Hoose (2009), Sensitivity studies of different aerosol indirect effects in mixed-phase clouds, *Atmos. Chem. Phys.*, *9*, 8917–8934, doi:10.5194/acp-9-8917-2009.

Lohmann, U., L. Rotstayn, T. Storelvmo, A. Jones, S. Menon, J. Quaas, A. M. L. Ekman, D. Koch, and R. Ruedy (2010), Total aerosol effect: Radiative forcing or radiative flux perturbation?, *Atmos. Chem. Phys.*, *10*(7), 3235–3246, doi:10.5194/acp-10-3235-2010.

Machenhauer, B., and I. Kirchner (2000), Diagnosis of systematic initial tendency errors in the ECHAM AGCM using slow normal mode data assimilation of ECMWF reanalysis data, *CLIVAR Exchanges*, *5*(4), 9–10.

Ming, Y., V. Ramaswamy, P. A. Ginoux, L. W. Horowitz, and L. M. Russell (2005), Geophysical Fluid Dynamics Laboratory general circulation model investigation of the indirect radiative effects of anthropogenic sulfate aerosol, *J. Geophys. Res.*, *110*, D22206, doi:10.1029/2005JD006161.

Morrison, H., and A. Gettelman (2008), A new two-moment bulk stratiform cloud microphysics scheme in the community atmosphere model, version 3 (CAM3). Part I: Description and numerical tests, *J. Clim.*, *21*(15), 3642–3659, doi:10.1175/2008JCLI2105.1.

Morrison, H., J. A. Curry, and V. I. Khvorostyanov (2005), A new double-moment microphysics parameterization for application in cloud and climate models. Part I: Description, *J. Atmos. Sci.*, *62*(6), 1665–1677, doi:10.1175/JAS3446.1.

Neale, R. B., et al. (2010), Description of the NCAR Community Atmosphere Model (CAM 5.0), *NCAR Tech. Note NCAR/TN-486 +STR*, Natl. Cent. for Atmos. Res., Boulder, Colo.

North, G. R., and M. J. Stevens (1998), Detecting climate signals in the surface temperature record, *J. Clim.*, *11*(4), 563–577, doi:10.1175/1520-0442(1998)011<0563:DCSITS>2.0.CO;2.

Park, S., and C. S. Bretherton (2009), The University of Washington shallow convection and moist turbulence schemes and their impact on climate simulations with the Community Atmosphere Model, *J. Clim.*, *22*(12), 3449–3469, doi:10.1175/2008JCLI2557.1.

Randall, D., M. Khairoutdinov, A. Arakawa, and W. Grabowski (2003), Breaking the cloud parameterization deadlock, *Bull. Am. Meteorol. Soc.*, *84*(11), 1547, doi:10.1175/BAMS-84-11-1547.

Rosenfeld, D., and G. Feingold (2003), Explanation of discrepancies among satellite observations of the aerosol indirect effects, *Geophys. Res. Lett.*, *30*(14), 1776, doi:10.1029/2003GL017684.

Rosenfeld, D., U. Lohmann, G. B. Raga, C. D. O'Dowd, M. Kulmala, S. Fuzzi, A. Reissell, and M. O. Andreae (2008), Flood or drought: How do aerosols affect precipitation?, *Science*, *321*(5894), 1309–1313, doi:10.1126/science.1160606.

Rotstayn, L. D., and J. E. Penner (2001), Indirect aerosol forcing, quasi forcing, and climate response, *J. Clim.*, *14*(13), 2960–2975, doi:10.1175/1520-0442(2001)014<2960:IAFQFA>2.0.CO;2.

Saha, S., et al. (2010), The NCEP Climate Forecast System Reanalysis, *Bull. Am. Meteorol. Soc.*, *91*, 1015–1057, doi:10.1175/2010BAMS3001.1.

Shine, K. P., J. Cook, E. J. Highwood, and M. M. Joshi (2003), An alternative to radiative forcing for estimating the relative importance of climate change mechanisms, *Geophys. Res. Lett.*, *30*(20), 2047, doi:10.1029/2003GL018141.

Stevens, B., and G. Feingold (2009), Untangling aerosol effects on clouds and precipitation in a buffered system, *Nature*, *461*(7264), 607–613, doi:10.1038/nature08281.

Twomey, S. (1977), Influence of pollution on shortwave albedo of clouds, *J. Atmos. Sci.*, *34*(7), 1149–1152, doi:10.1175/1520-0469(1977)034<1149:TIOPOT>2.0.CO;2.

Wang, M., et al. (2011a), The multi-scale aerosol-climate model PNNL-MMF: Model description and evaluation, *Geosci. Model Dev.*, *4*(1), 137–168, doi:10.5194/gmd-4-137-2011.

Wang, M., S. Ghan, M. Ovchinnikov, X. Liu, R. Easter, E. Kassianov, Y. Qian, and H. Morrison (2011b), Aerosol indirect effects in a multi-scale aerosol-climate model PNNL-MMF, *Atmos. Chem. Phys.*, *11*(11), 5431–5455, doi:10.5194/acp-11-5431-2011.

Wang, M., et al. (2012), Strong constraints on cloud lifetime effects of aerosol using satellite observations, *Geophys. Res. Lett.*, *39*, L15709, doi:10.1029/2012GL052204.

Wielicki, B. A., B. R. Barkstrom, E. F. Harrison, R. B. Lee III, G. L. Smith, and J. E. Cooper (1996), Clouds and the Earth's Radiant Energy System (CERES): An Earth observing system experiment, *Bull. Am. Meteorol. Soc.*, *77*, 853–868, doi:10.1175/1520-0477(1996)077<0853:CATERE>2.0.CO;2.

Wood, R. (2007), Cancellation of aerosol indirect effects in marine stratocumulus through cloud thinning, *J. Atmos. Sci.*, *64*(7), 2657–2669, doi:10.1175/JAS3942.1.

Zhang, G. J., and N. A. McFarlane (1995), Sensitivity of climate simulations to the parameterization of cumulus convection in the Canadian climate center general-circulation model, *Atmos. Ocean*, *33*(3), 407–446, doi:10.1080/07055900.1995.9649539.